

2017-01-26

Innovative tidal notch detection using TLS and fuzzy logic: Implications for palaeo-shorelines from compressional (Crete) and extensional (Gulf of Corinth) tectonic settings

Schneiderwind, S

<http://hdl.handle.net/10026.1/8424>

10.1016/j.geomorph.2017.01.028

Geomorphology

Elsevier BV

All content in PEARL is protected by copyright law. Author manuscripts are made available in accordance with publisher policies. Please cite only the published version using the details provided on the item record or document. In the absence of an open licence (e.g. Creative Commons), permissions for further reuse of content should be sought from the publisher or author.

Note: This is the author version of the paper and may not reflect changes made to the final version of record available at <http://dx.doi.org/10.1016/j.geomorph.2017.01.028> © 2017. This manuscript version is made available under the CC-BY-NC-ND 4.0 license <http://creativecommons.org/licenses/by-nc-nd/4.0/>

Innovative tidal notch detection using TLS and fuzzy logic: implications for palaeo-shorelines from compressional (Crete) and extensional (Gulf of Corinth) tectonic settings

Schneiderwind, S.^{a,*}, Boulton, S.J.^b, Papanikolaou, I.^c and Reicherter, K.^a

a) Institute of Neotectonics and Natural Hazards, RWTH Aachen University, Lochnerstraße 4-20, 52056 Aachen, Germany. Email: s.schneiderwind@nug.rwth-aachen.de

b) School of Geography, Earth and Environmental Sciences, Plymouth University, Plymouth, Devon PL4 8AA, UK.

c) Laboratory Mineralogy – Geology, Agricultural University of Athens, Iera Odos 75, 11855 Athens, Greece.

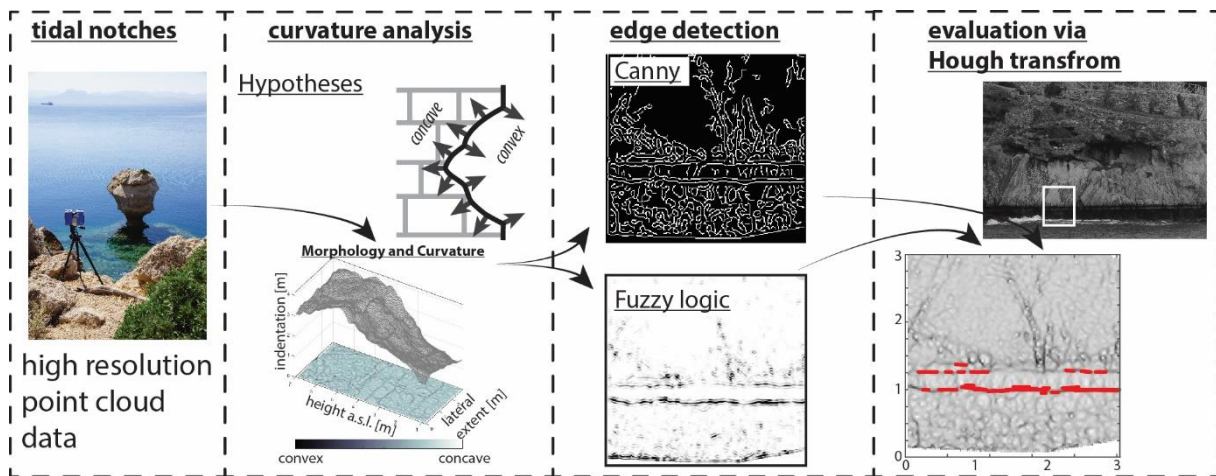
*Corresponding author. Tel: +49 (0) 241 80-95722; Fax: +49 (0) 241 80-92358.

E-mail address: s.schneiderwind@nug.rwth-aachen.de (S. Schneiderwind)

Abstract

Tidal notches are a generally accepted sea-level marker and maintain particular interest for palaeoseismic studies since coastal seismic activity potentially displaces them from their genetic position. The result of subsequent seismic events is a notch sequence reflecting the cumulative coastal uplift. In order to evaluate preserved notch sequences, an innovative and interdisciplinary workflow is presented that accurately highlights evidence for palaeo-sea-level markers. The workflow uses data from terrestrial laser scanning and iteratively combines high-resolution curvature analysis, high performance edge detection, and feature extraction. Based on the assumptions that remnants, such as the roof of tidal notches, form convex patterns, edge detection is performed on principal curvature images. In addition, a standard algorithm is compared to edge detection results from a custom Fuzzy logic approach. The results pass through a Hough transform in order to extract continuous line features of an almost horizontal orientation. The workflow was initially developed on a single, distinct, and sheltered exposure in southern Crete and afterwards successfully tested on laser scans of different coastal cliffs from the Perachora Peninsula. This approach allows a detailed examination of otherwise inaccessible locations and the evaluation of lateral and 3D geometries, thus evidence for previously unrecognised sea-level markers can be identified even when poorly developed. High resolution laser scans of entire cliff exposures allow local variations to be quantified. Edge detection aims to reduce information on the surface curvature and Hough transform limits the results towards orientation and continuity. Thus, the presented objective methodology enhances the recognition of tidal notches and supports palaeoseismic studies by contributing spatial information and accurate measurements of horizontal movements, beyond that recognized during traditional surveys. This is especially useful for the identification of palaeo-shorelines in extensional tectonic environments where coseismic footwall uplift (only 1/2 to 1/4 of net slip per event) is unlikely to raise an entire notch above the tidal range.

Keywords: Tidal notches; Terrestrial laser-scanning; Computer vision; Fuzzy logic; Hough transformation; Palaeoseismology.



1. Introduction

In microtidal seas, such as the Mediterranean, tidal notches can be used to derive and quantify relative coastal movements during the Holocene (Pirazzoli, 1991). To develop these prominent strandlines, ranging from a few centimetres to several metres deep, the sustained action of physical, chemical, and biological erosion within the tidal range is necessary. Therefore, exposure to wave action, lithologic resistance to quarrying, and the strength of the rock able to support the weight of the overburden are key parameters effecting the shape of resultant notches (Trenhaile, 2015). In tectonically active regions, these distinct ecological and morphological features define the modern shoreline, and when equivalent older features are different from the present-day sea-level coseismic activity can be inferred (Fig. 1) (i.e., Boulton and Stewart, 2015). However, a direct correlation of individual sea-level markers to palaeoearthquake parameters is an outstanding challenge especially in extensional tectonic settings. For example, the shoreline of western Crete was uplifted by up to 9 m during the compressional M 8.5 Hellenic earthquake in 365 A.D., forming a classic example for a lifted prominent strandline as a consequence of rapid emergence (Shaw et al., 2008). This distinct palaeoshoreline is well-preserved and has not been affected by wave attack or midlittoral erosion. By contrast, shorelines that experienced rapid emergence due to extensional tectonic movements, such as those from Perachora Peninsula in the Gulf of Corinth, are not likely to preserve fully developed tidal notches. In these settings, the amount of coseismic displacement is usually up to an order of magnitude lower than in megathrust events, and moreover the uplift component is estimated to be only 1/4 to 1/2 of the net slip per earthquake (e.g. Armijo et al., 1996; McNeill et al., 2005; Papanikolaou et al., 2010) and thus not likely to exceed the tidal range of ~ 0.4 m in the Mediterranean Sea (Evelpidou et al., 2012). Therefore, it is suggested that apparent notches reflect the cumulative effect of multiple seismic events and individual notch levels cannot usually be attributed to specific earthquakes in regions of tectonic extension (e.g. Stewart and Vita-Finzi, 1996; Cooper et al., 2007; Boulton and Stewart, 2015). The identification of a palaeoshoreline is, among bioerosional remnants or consolidated beach deposits, based on the recognition of distinct erosional marks of former midlittoral zones (Pirazzoli et al., 1994). Typically, the notch position is mapped on a 1:5000-scale map (Cooper et al., 2007) and measurements are made to create morphometric profiles. Profiles are usually collected by tape measure (e.g. Kershaw and Guo, 2001) and include the average vertical extent of a notch and the maximum indentation (e.g. Antonioli et al., 2015). Vertical sheltered coasts are preferred for precise

notch measurements (Pirazzoli, 1986), yet often these cliffs are inaccessible, and for that reason mid-range profiling using a handheld laser distance meter allowing evaluation of inaccessible and dangerous cliffs has also been employed (Kázmér and Taboroši, 2012). To address morphometric variations, a structure-from-motion (SfM) approach is also presented by Bini et al. (2014), which produces high resolution 3D models from a surface using a series of overlapping photographs.

The problem of lateral profile heterogeneity is extensively discussed by Kershaw and Guo (2001), demonstrating that active fault segments crossing cliffs, local variations of different wave and surf regime, and/or bedrock heterogeneity result in different notch profiles even in nearby sites (see also Evelpidou et al., 2012). Furthermore, collecting multiple profiles manually is time consuming and contains potential error sources. For instance, the correlation of different extracted levels from morphometric profiles is challenging and requires a constant reference datum over the time period of profile collection. We suggest that terrestrial laser scanning (TLS) provides all requirements for palaeoseismological studies on emerging coasts. The data are of high precision and resolution, and enables the analysis of the surface curvature of a whole cliff in a reasonable amount of time.

This paper aims to present an interdisciplinary study of computer vision and palaeoseismology. High resolution data from TLS is investigated utilising multiscale image analysis and semi-automatic edge detection. Conventional gradient analysis is compared to modern modelling from Fuzzy logic methodology. Afterwards, feature extraction by Hough transformation gives spatial evidence for the existence of tidal notches within an entire sequence of palaeo-strandlines on a cliff.

In their comprehensive analysis of tidal notches in the Mediterranean, Antonioli et al. (2015) concluded that notch formation processes have not changed during the last 125 kyrs. Similar widths of both last interglacial and modern notches suggest equivalent tidal ranges as zones of notch formation. Hence, the retreat zone of a tidal notch representing mean sea-level can be inferred by knowing the local tidal amplitude and the position of either roof or floor. Particularly in the Mediterranean, the use of tidal notches as palaeo-sea-level markers to determine rates of tectonic activity is widespread, since potential errors are limited by low tidal ranges and the lack of strong waves (Pirazzoli and Evelpidou, 2013). Therefore, the coastline at Perachora Peninsula in the eastern Gulf of Corinth provides suitable conditions to apply an innovative method improving tidal notch identification and comparison on local and regional scales. In order to verify and calibrate the method, which focusses on changing curvature at the roof or bottom of a notch, a distinct tidal notch in southwestern Crete ~1 m above recent sea-level uplifted by the 365 A.D. earthquake (Shaw et al., 2008) is investigated as reference model.

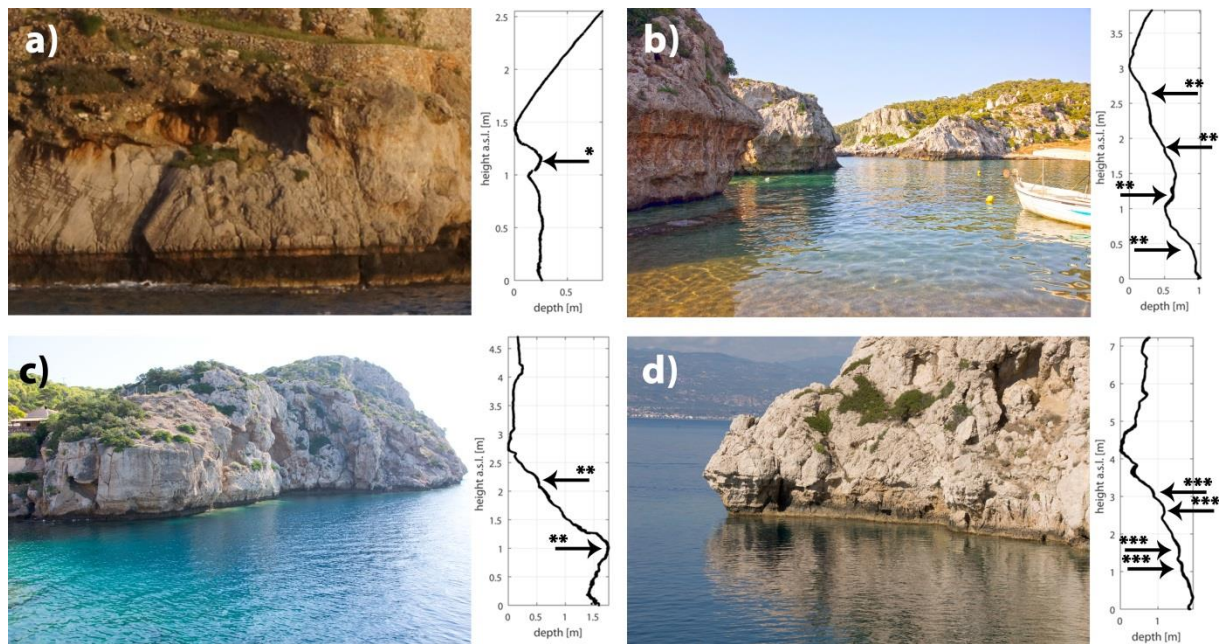


Fig. 1. Collage of raised shorelines on Crete and Central Greece and associated notch profiles extracted from TLS data. The tidal notch at Agios Pavlos (a) was raised by the 365 A.D. earthquake and forms the reference for notch detection (* Shaw et al., 2008). Exposures at the coast of Perachora Peninsula (Gulf of Corinth) are known from literature (** Kershaw and Guo, 2001; *** Pirazzoli et al., 1994) and pose testing targets in this study: b) Mylokopy Bay; c) Heraion Harbour, and d) Heraion Lighthouse.

2. Study sites

2.1. Agios Pavlos, SW Crete

The island of Crete is directly adjacent to the Hellenic subduction zone between Europe and Africa (Fig. 2) and comprises a complex geological and tectonic structure that results from successive thrusting of alpine geotectonic units and the activity of major detachment faults. Crustal extension orientated both arc-parallel and arc-perpendicular has led to the development of Quaternary carbonate bedrock fault scarps throughout the island (Caputo et al., 2010). These normal faults mainly juxtapose Mesozoic carbonates of the Pindos unit in their footwall against hanging-wall flysch and /or post-alpine sediments. Vertical tectonic movements along the western part of the island are associated with both fault populations, causing earthquakes along the nearby Hellenic trench and on normal faults onshore. As a result, clearly visible emerged shorelines are developed on the limestone cliffs. The 365 A.D. earthquake rapidly uplifted the well indented strandline by ~1 m at Agios Pavlos, located approximately 70 km eastwards from the activated structure and evidences the recent regional uplift phase (Stiros, 2010). Crete has experienced ~2.5 km of uplift since the Early Tortonian (Miocene) in several different phases (Meulenkamp et al., 1994). The most recent phase of uplift, as evidenced by uplifted Messinian deposits (Krijgsman, 1996), began at around 6 Ma and continues to the present day. The study location is located inside a 200 m wide bay and is protected from rough seas in accordance with official nautical cartographies and data from oceanographic buoys (<http://utmea.enea.it/energiadalmare/>).

132
133
134
135
136
137
138
139
140
141
142

143
144
145
146

147
148
149
150
151
152
153

154
155
156
157
158
159
160

2.2. *Perachora Peninsula, eastern Gulf of Corinth*

North-South directed extension with rates of 10–15 mm yr⁻¹ makes the Gulf of Corinth one of the most rapidly extending areas on Earth. Along the southern shore of the graben are active north-dipping normal faults uplifting coastal regions in the footwall. Rates of fault motion lie in the range of 1–10 mm yr⁻¹ and are evidenced by Quaternary and Holocene palaeoshorelines (Armijo et al., 1996; Morewood and Roberts, 1999; Cowie and Roberts, 2001; McNeill and Collier, 2004; Leeder et al., 2003; Cooper et al., 2007; Roberts et al., 2009). Leeder et al. (2005) estimate slip rates of ~2.5 mm yr⁻¹ for normal faulting structures in the Alkyonides Gulf and the Perachora Peninsula over a period of 0.6 Myrs (Fig. 2). However, the authors also postulate that onshore faults (Schinos and Pisias) are more active than parallel offshore structures.

The coastline of the Perachora Peninsula is predominantly comprised of Mesozoic and Pleistocene carbonates. In some parts of the southwestern part of the peninsula, a thin composite volcanosedimentary series of basic rocks occurs. Occasionally, marine deposits of Tyrrhenian age comprising conglomerates crop out along northern coastlines (Bornovas et al., 1984).

The Heraion archaeological site is located at the northwestern tip of the Perachora Peninsula (Fig. 2b). The tidal notches at this site are described by several authors. Pirazzoli et al. (1994) identified four raised notches at the lighthouse between +1.1 and +3.2 m and dated them to 4.4–4.3 kyrs BP (+3.2 m), 2.4–2.2 kyrs BP (+2.6 m), and 0.4–0.2 kyrs BP (+1.1 m) (see Fig. 1). Kershaw and Guo (2001) tried to correlate these notches to exposures at the harbour of Heraion only a few hundreds of metres to the east (+0.75 and +2.05 m). The authors conclude that differential uplift on cross-cutting faults causes dislocations of former strandlines and prevents a correlation between the two sites.

Another site mentioned by both studies is located along the northern shore of the peninsula. The Mylokopy beach actually consists of two small bays, separated by a tombolo. At the tip of the tombolo a massive limestone block contains up to five notch generations, which vary in height from the surrounding cliffs because of fault activity. In addition, three different notch morphometric profiles (identified notches at +0.4, +1.2, +2.0, and +2.6 m) can be extracted due to varying exposure to the sea and abrasional components (Kershaw and Guo, 2001).

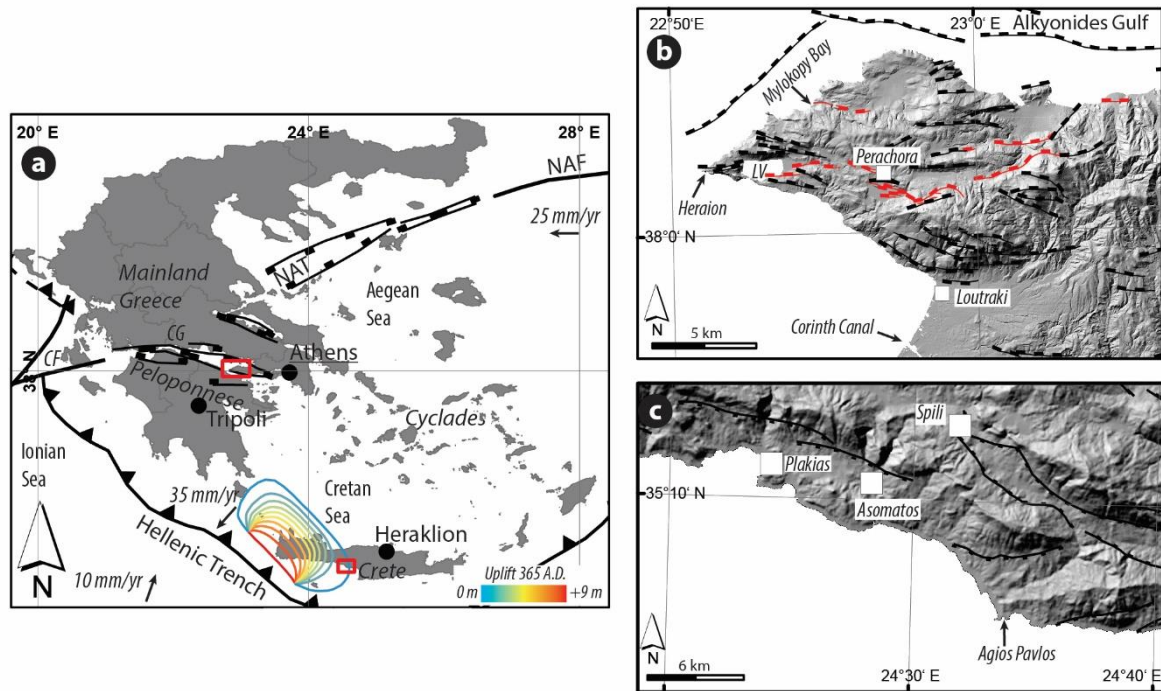


Fig. 2. Overview map of studied sites. a) Map of Greece showing simplified large-scale tectonic structures (CG, Corinthian Gulf; CF, Cephalonia Fault; NAF, North Anatolian Fault; NAT, North Aegean Trough; black lines with barbs show active thrusts; black lines with marks show active faults) (after Papanikolaou and Royden, 2007; Shaw et al., 2008). Red boxes highlight study areas. b) DEM (from 10m contour lines) of the Perachora Peninsula. Red lines with marks indicate normal faults that have been activated during the 1981 earthquake sequence (Bornovas et al., 1984). LV, Lake Vouliagmeni. c) DEM (SRTM-1) of the southwestern coast of Crete. The morphology indicates tectonic structures (black line with marks) that potentially down-throw coastal areas (Bonneau, 1985).

3. Methodology

The methods presented include data acquisition from TLS and processing for semi-automated edge detection based on the surface curvature of a cliff. One scan from the distinct shoreline at Agios Pavlos operates as a reference for a unique tidal notch at this particular cliff, since the 365 A.D. thrust event raised the strandline > 1 m from the erosional zone. Thus, we assume this exposure is not affected by ongoing erosion. Consequently, the method is developed from this exposure and then tested on sites from the Perachora Peninsula.

3.1 Theoretical assumptions

The term tidal notch refers to a horizontal erosion feature formed at sea-level due to coeval action (Antonioli et al., 2015) of chemical, physical, and biological factors (Pirazzoli, 1986). However, the predominant agent is commonly assumed to be bioerosion (Evelpidou et al., 2012), which is restricted to carbonate rocks. Well-defined vegetational belts are the result of different grazing or boring organisms each living in individual horizontal galleries. Therefore, Pirazzoli (1986) suggested a vertical zonation (Fig. 3a) for notches, which also indicates maximum erosional potential at mean sea-level (Fig. 3b). Moreover, the classical symmetrical notch profile (e.g. Laborel et al., 1999; Trenhaile, 2015)

is formed of three main sections (Fig. 3): I) A floor or base which extends to the limit of permanent immersion at tidal low stand; II) a retreat zone of maximum concavity exhibiting the inflection point near mean sea-level, and III) a roof near high tide level.

In an area of extensional tectonics, such as the Gulf of Corinth, the ratio of footwall uplift to hanging-wall subsidence is estimated to 1/4 to 1/2 where the total net slip is not likely to exceed ~2 m, since normal faulting structures usually do not produce earthquakes > M 7.0 (e.g. Jackson et al., 1982; Stewart and Vita-Finzi, 1996; Papanikolaou et al., 2010). Offshore, but close to the coast, normal faulting seismic activity causes rapid emergence of coastal cliffs; however, coseismic uplift exceeding the tidal range of ~0.4 m is unlikely since it would require minimum mean displacements of 1.6 ± 0.4 m (based on Wells and Coppersmith, 1994; for M 6.5–7.0 empirical maximum displacements range from 0.8 to 2.1 m) which are unrealistic values of surface faulting for the vast majority of normal faulting earthquakes. Thus, the former and new erosional zone along the cliff would overlap, overprinting the earlier notch (Fig. 3b). Pirazzoli (1986) labels features of this origin as ‘ripple notches’. However, depending on the time and vertical displacement, the resulting shape is tantamount to a widened single notch; due to the tidal range variation. Only at close range minor variations will be detectable on the surface curvature and normal to the orientation of the roof (Fig. 3c).

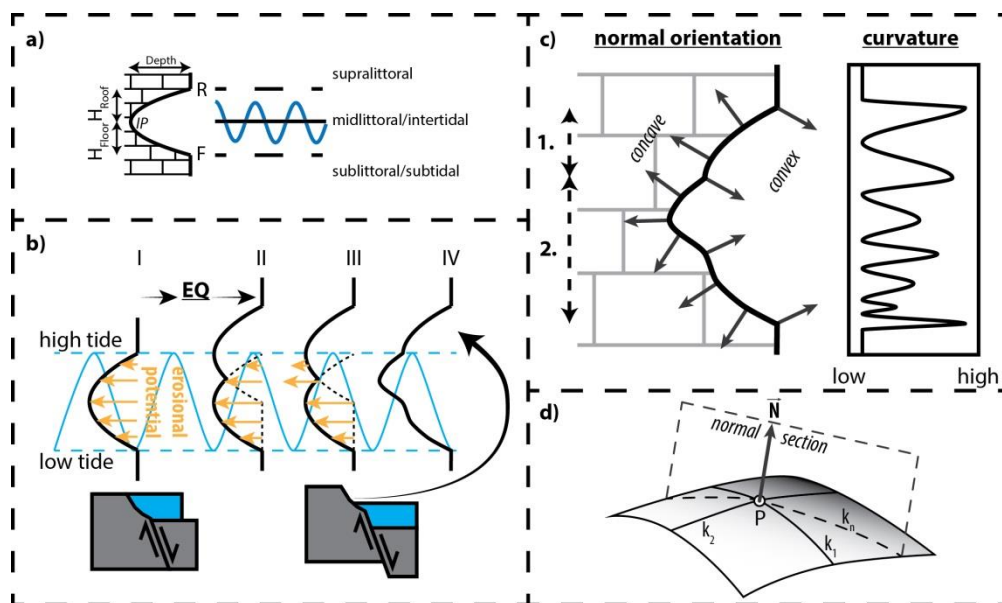


Fig. 3. Theoretic assumptions. a) Zonation of a simplified tidal notch (R, roof; F, floor; IP, inflection Point) following suggestions of Pirazzoli (1986). b) Evenly distributed erosional potential pointing at mean sea-level causes a symmetrical shape of a tidal notch (I). When the erosional zone gets offset by an earthquake (II–IV), the level-based erosional potential attacks the prior to this created cliff morphology (III). The resulting shape comprising two notch generations (1 and 2) exhibits patterns of convex or concave curvature (c). d) Visualisation of the estimate of the normal vector (N) at any point (P) along a normal section from principal curvatures k_1 and k_2 .

3.2 TLS

Terrestrial laser scanning (TLS) is a commonly used remote sensing technique with a high spatial and temporal resolution and is highly effective for reconstructing morphology (Wilkinson et al., 2015), interpreting trenches and outcrops (Schneiderwind et al., 2016), monitoring movements (Rosser et al., 2013), extracting slip vectors (Jones et al., 2009), and recording smoothness along fault planes (Wiatr et al., 2015).

The fundamental principle underlying TLS is rapid measurement of one-dimensional distances using a model-specific wavelength within the electromagnetic spectrum. A coherent laser beam with little divergence propagates dominantly in a well-defined direction and is reflected off surfaces, forming a non-contact and non-penetrative active and stationary recording system. Most common are systems that make use of the time-of-flight principle, where the instrument measures the time delay between emission, reflection and receiving the laser pulse. Phase-based TLS bypass the requirement of a high-precision clock by modulating the power of the laser beam and measuring the phase difference between the emitted and received waveforms (Smith, 2015). The result is an irregular but dense point cloud (x,y,z coordinates) representing a highly detailed digital 3D surface model. In both systems, the data quality is controlled by the range between sensor and target, surface properties (e.g. moisture, roughness), and also the angle of incidence.

In this study we used a time-of-flight mode operating Optech ILRIS 3D system for scans collected on Crete and a Faro Focus 3D system (phase-based mode) during the survey in central Greece due to logistical constraints. All scans were undertaken during calm sea conditions and from close-range to mid-range (max. 100 m). In order to correlate the data from multiple sites at the Perachora Peninsula, hourly tide gauge data from the Posidonia station (Hellenic Navy Hydrographic Service) was applied to the individual point clouds referenced to mean sea-level (Fig. 4).

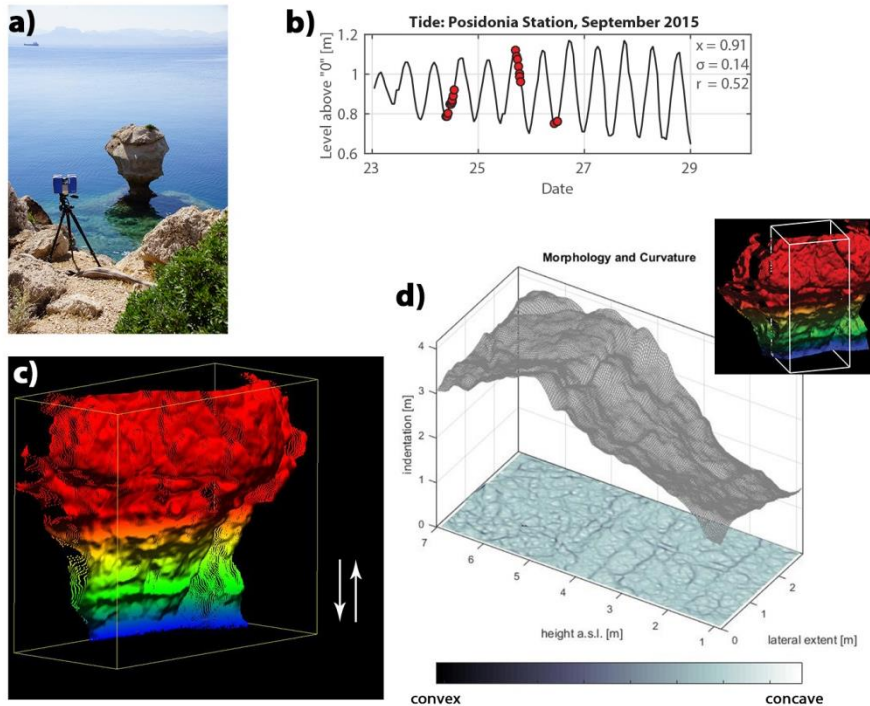


Fig. 4. Data acquisition and processing. a) Close- to mid-range laser scanning. b) Tide gauge data provided by the Hellenic Navy Hydrographic Service (\bar{x} = mean sea-level, σ = standard deviation, r =

tidal range) from the moment of scanning (red dots). c) High resolution point cloud data adjusted to mean sea-level using the tide gauge data as a reference datum. d) Segments prepared for surface curvature analysis (d). Extraction of two-dimensional information about the surface curvature reduces error sources from interpreting 3D surfaces.

Once the point clouds are corrected for their individual spatial information, principal curvature analysis is performed. In general, curvature is the second derivative of a function $f(x)$ and describes the amount by which a geometric object differs from being flat. Depending on the sign, the object is either convex or concave at any point P , and the surface normal \vec{N} is oriented perpendicular to the surface towards maximum curvature. The magnitude k of difference from a flat object is quantitatively described by:

$$k = \frac{f''(x)}{[1+(f'(x))^2]^{\frac{3}{2}}} \quad (1)$$

The mean curvature at a point on a third dimension uses both the maximum and minimum normal curvatures. These principal curvatures are orientated mutually perpendicular with $k_1 > k_2$ (Fig. 3d). However, since tidal notches are a horizontal sea-level marker, only the vertical principal curvature is respected for the analysis. Moreover, the minimum curvature k_2 highlights exclusively convex patterns corresponding to features such as the roof of a tidal notch. This automatically excludes sources of misinterpretation (e.g. joints or cracks) and focuses on horizontal differences (Fig. 4d).

To calculate the surface curvature, TLS data provides surface information with x , y , z coordinates, where the z -coordinate describes the lateral indentation value. To sharpen the principal curvature information, standard averaging and 2D median filtering are applied.

3.3 Edge detection

The curvature defines a parameter essential for curve sketching. However, this value does not have a primary link to neighbourhood relationships. Indeed, the curvature at any point is calculated from the adjacent points but it does not quantify geometric alignments, such as straight edges, and the curvature of neighbouring pixels is not compared. Therefore, methods of edge detection are applied which aim to identify points where abrupt changes and discontinuities in the surface curvature occur. Furthermore, the process reduces the curvature plot to its significant details that appear as convex objects.

3.3.1 Canny method

Edge detection is an integral part of many computer vision systems and multiscale image analysis. The method results in a dramatic reduction of processed data, while preserving structural information about object boundaries (Canny, 1986). In general, an image contains edges where the gradients along the x - or y -axis show rapid changes in image intensity. For instance, the transition from black to white (which equals the values of 0 and 255 in an 8-bit array) within just two pixel cells depicts a sharp edge with the highest possible gradient. Ideally, the result is a binary image that only contains information

about edges within the initial intensity image. To decide whether an edge is located at a certain part of the image, one of the following criteria has to be fulfilled:

- a) The first derivative of the intensity is larger in magnitude than a given threshold; or
- b) The second derivative of the intensity has a zero-crossing (i.e. where the intensity of the image changes rapidly or the first derivative changes sign).

The built-in MatlabTM edge function provides several estimators that implement these rules. Furthermore, sensitivity for horizontal over vertical edges can be applied. The Canny edge detector has become standard in edge detection by defining two thresholds for strong and weak edges, respectively. Technically, the algorithm applies a Gaussian noise reduction and a non-maximum suppression to eliminate multiple responses. Edges classified as weak only persist in the resulting binary image when these are connected to strong edges. Therefore, the three criteria of edge detection (good detection, good localization, and low spurious response) are addressed (Canny, 1986; Bao et al., 2005).

3.3.2 Fuzzy logic

Zadeh (1965) described a fuzzy set as a class of objects without a precisely defined criterion of membership. Within a fuzzy set each object is assigned to a grade of membership ranging between zero and one. Hence, approaches for decision-making (Bellman and Zadeh, 1970) and cluster analysis (Bezdek and Harris, 1978) were developed. Translated to edge detection from surface curvature the Fuzzy logic approach allows the use of membership functions to define the degree at which a pixel belongs to a convex edge or a different region. This is also the essential statement defining the membership function. Therefore, other than from the Canny edge detector, the result is an intensity image and not a binary type. Consequently, edge detection and recognition still belongs to the user and is not the result of any blackbox approach securing transparency in the process.

Edge detection using Fuzzy logic comprises three steps. Firstly, directional gradients (G_x , G_y) and gradient magnitudes (Mag_x , Mag_y) serve as input information for a fuzzy set and have to be obtained from the curvature plot using the Prewitt gradient operator (Fig. 5). The Prewitt operator is a standard edge detection algorithm that accurately highlights vertical or horizontal alignments (Zhang et al., 2013) (Fig. 5b). Secondly, a fuzzy inference system (FIS) specifies a zero-mean Gaussian membership function for each input where the range of directional magnitudes depicts the limiting range values (Fig. 5c). If the gradient value is zero the pixel belongs to the zero membership function of grade 1. The grade along function quantifies the degree of membership of a certain element to the fuzzy set. In order to adjust the sensitivity of edge detection, multiples of standard deviation (s_x , s_y) of both zero membership inputs control the edge detector performance. Because of the high resolution of TLS data and dense point cloud, those values should be >1 to decrease sensitivity for areas of minor interest (e.g. small cracks or joints). Furthermore, defining $s_x \gg 1$ encompasses the majority of plan curvature within the zero-membership function and thus excludes those from analysis. Therefore, a triangular membership function is specified for the output intensity image. Start, peak, and end of the triangles influence the intensity of the detected edges and can be adjusted as required to improve edge detection performance.

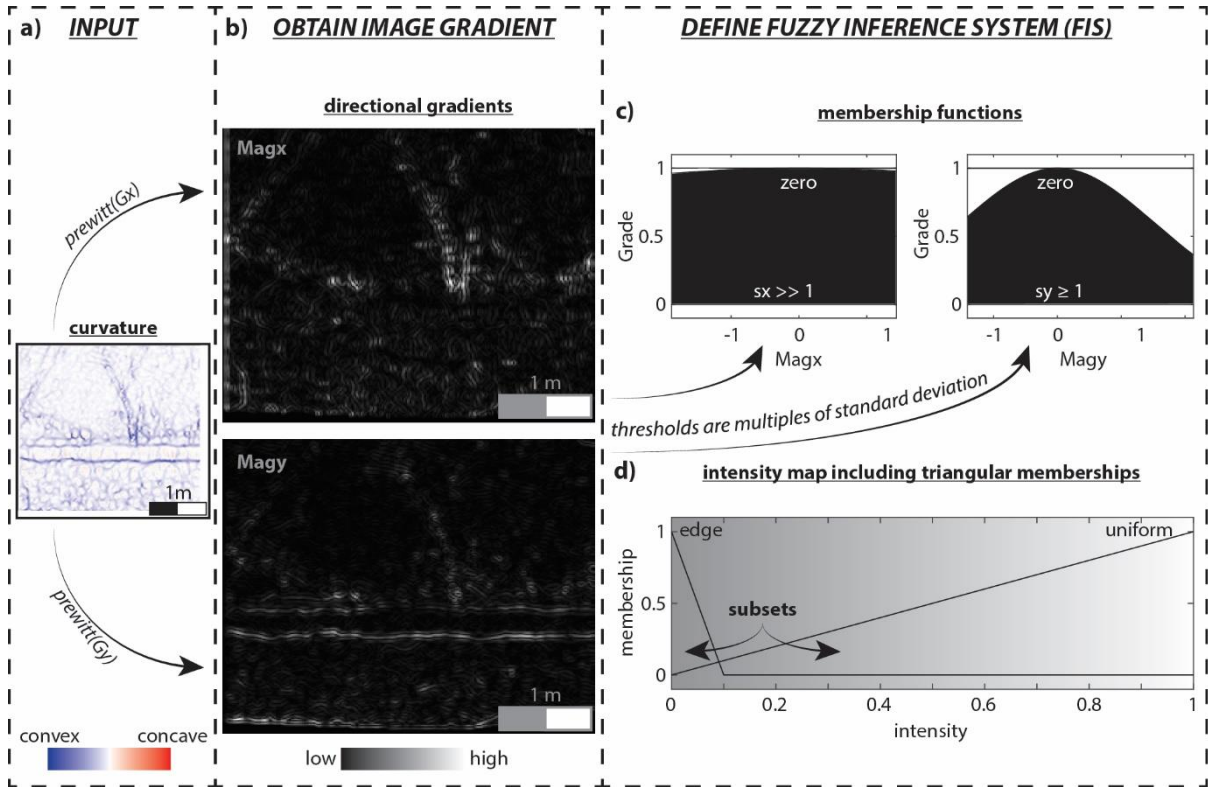


Fig. 5. Fuzzy set edge detection. Edge detection is performed on principal curvature images (a). Two-dimensional gradients (b) are individually addressed in defined membership functions (c). The intensity map (d) shows subsets of different memberships. White pixels belong to a uniform region; only very dark pixels represent detected edges (Fig. 6c).

The third step of edge detection from Fuzzy logic includes rule specification and evaluation of the FIS. For classification of the intensity map, two rules are necessary which access three simple principles of set theory (If-then, AND, OR):

- If Mag_x is zero and Mag_y is zero then intensity is white
- If Mag_x is not zero or Mag_y is not zero then intensity is black

By this formulation a pixel of gradient different from zero depicts black and belongs to an edge (Fig. 6). Furthermore, the gradient is defined to be zero by Gaussian membership functions and forms the input for the applied FIS.

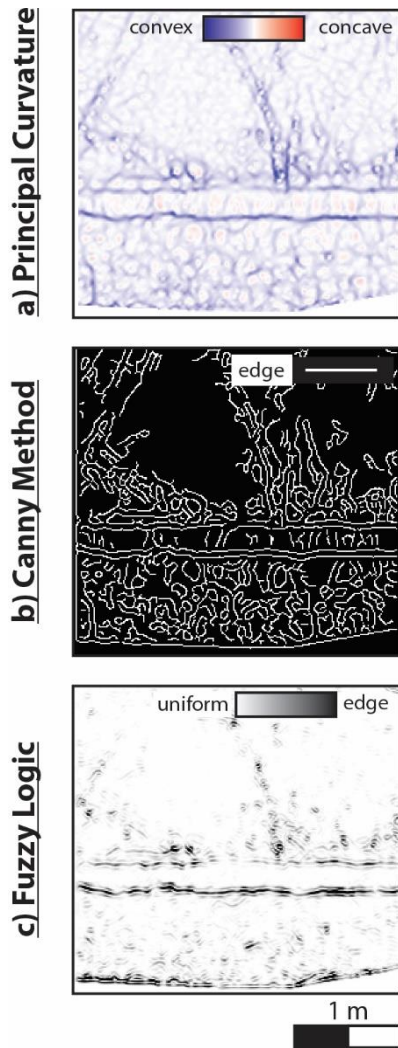


Fig. 6. Comparison of applied analyses. a) Principal curvature depicting a high resolution image of the cliff morphology. b) Edge detection after Canny. It is successful in notch detection but also highlights small edges of minor interest. c) Edge detection from Fuzzy logic, highlighting rapidly changing gradients in a horizontal manner.

3.4 Hough transform

The Hough transform is a popular tool for feature detection due to its robustness to noise (Fernandes and Oliveira, 2008). The technique aims to find imperfect instances of objects representing line features by a voting procedure. For this procedure image objects are compared to the parametric term of a straight line. For some technical reasons, it is proposed to use its Hesse normal form since vertical lines would give rise to unbounded values of the slope (Duda and Hart, 1972):

$$\rho = x \cos \theta + y \sin \theta \quad (2)$$

where the variable ρ is the distance from the origin (0,0) to the line along a vector perpendicular to the line, and θ is the angle between the x-axis and this vector with a range of $-90^\circ < \theta < 90^\circ$. Thus, the gradient of a line feature is the tangent of $90 - \theta$. The result of the Hough transformation is a parameter space matrix comprising ρ and θ vectors for each pixel (x, y) , where the algorithm determines evidence

of a straight line with respect to neighbouring pixels. Furthermore, it depicts a voting map [0 1] representing the discretised parameter space of detected objects (Fernandes and Oliveira, 2008). Local maxima (peaks) in this map represent parameters (ρ , ϑ) of the most likely lines that can be extracted.

Since the Matlab™ Hough function requires a binary image input, the intensity map from Fuzzy Logic edge detection is converted using a global image threshold (Otsu, 1979). Beside that, line segment extraction from the Hough transform follows the same workflow for both data sets from edge detection (Canny Method and Fuzzy Logic) (Fig. 7). After the Hough transform is computed, peak values in the voting map are identified, where the user specifies the number of peaks to identify and thus, controls the influence of minor objects.

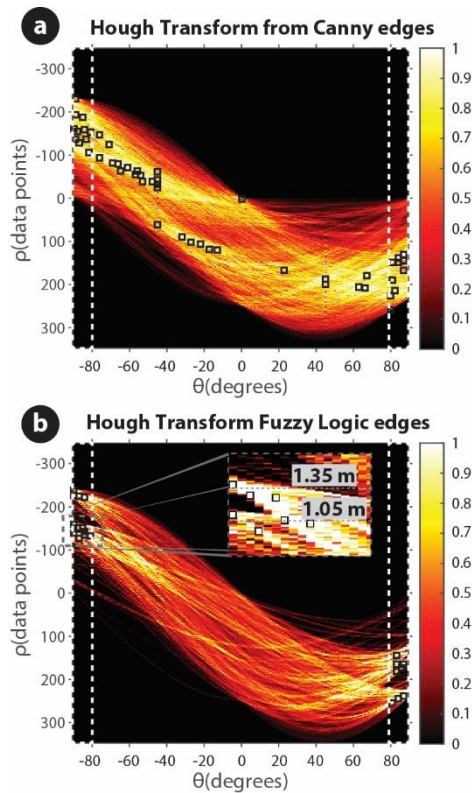


Fig. 7. Hough transform from detected edges. Dashed areas indicate potential line features with absolute $\vartheta > 80^\circ$. Due to its sensitivity, extracted line segments from Canny edge detector (a) are more spread and randomly orientated than from Fuzzy Logic edge detection (b). Peaks in the normalised voting map (squares) represent parameters for most likely lines. Zoom indicates to peak cluster of almost horizontal oriented line features corresponding to elevations of the notch's roof and floor, respectively.

4. Results

4.1. Developing methods, Agios Pavlos, Crete

The workflow was developed utilising curvature analysis, edge detection using a Canny algorithm, a Fuzzy logic approach, and Hough line extraction on laser scan data from Agios Pavlos. The principal curvature analysis clearly highlights convex patterns (Fig. 6a) as expected from theoretical assumptions

(Fig. 3). The prominent strandline is obviously defined by an evenly convex roof and floor. However, not only horizontal asperities resulting from erosion at sea-level are registered. In order to reduce the image information and to focus on almost horizontal and continuous features, two individual edge detection approaches were applied. The conventional Canny edge detector predicts sharp changes in surface curvature suitable for the roof and the floor of the notch. Furthermore, minor morphological irregularities are ignored and not interpreted as a discontinuity. However, the algorithm does not sufficiently exclude information from plan curvature and consequently omits edges from features of minor interest, such as joints, cracks or weathering aspects (Fig. 6b). The Canny edge detector returns a bivalent set of uniform areas and edges and thus, does not differ for gradual irregularities within the subset "edge". Consequently, only the predominant horizontal orientation of edges detected at the extents of the notch is evidence for its existence. The membership functions of the Fuzzy logic approach allow outputs of quasi-probabilistic edge occurrence (Fig. 6c). This means detected edges, which are almost the same as from the Canny detector, are ranked towards the grade of conformance with formulated rules. Furthermore, focus is complied with horizontal features reducing image information once more towards the recognition of sea-level marker.

The Hough transform returns a matrix of a discretised parameter space displayed as a graph of line feature distance from the origin (ρ) against line feature deviation from vertical (ϑ). Fig. 7 contrasts the resulting matrices from Canny edges with edges determined from Fuzzy logic. It is obvious that peaks and hot spots representing accumulations of ρ , ϑ -pairs are wider spread when Canny edges determine the input for Hough transform. Especially from ϑ -values distributed edge orientations are confirmed (see also Fig. 6b). However, for almost horizontal line features the corresponding absolute ϑ -value should be $> 80^\circ$, since it represents the normal vector orientation. When edges determined from the Fuzzy logic approach are input for the Hough transform the resulting peaks are clustered at highest ϑ -values. Furthermore, hot spots are clearly separated from each other and enable correlation to corresponding heights in the laser scan (Fig. 7b). Peaks located at minimum or maximum ρ -values correspond to the upper or lower image extent. The laser scan at Agios Pavlos shows some minor wave action resulting in a lack of data in the lower part of the cliff section and causing detected edges and determined line features in this region (Fig. 8).

When comparing the results of line feature determination from different inputs, it is conspicuous how spread peaks in the parameter space influence the focus on distinct morphological features. Line structures extracted from Canny edges do not represent the roof and floor of the notch exclusively. Lines following edges from generic irregularities, such as those from weathering in the lower parts, are also extracted. Indeed, features with ϑ -values $< 80^\circ$ can be suppressed in the plot (see Fig. 8b) but this still does not provide a threshold for distinct features. Due to the membership functions of the Fuzzy logic approach gradual distinction of edge detection enables adjustment of such thresholds. As a result, only the notch at ~ 1.2 m is highlighted (Fig. 8c). Therefore, it seems the identification of tidal notch morphologies on coastal cliffs is possible.

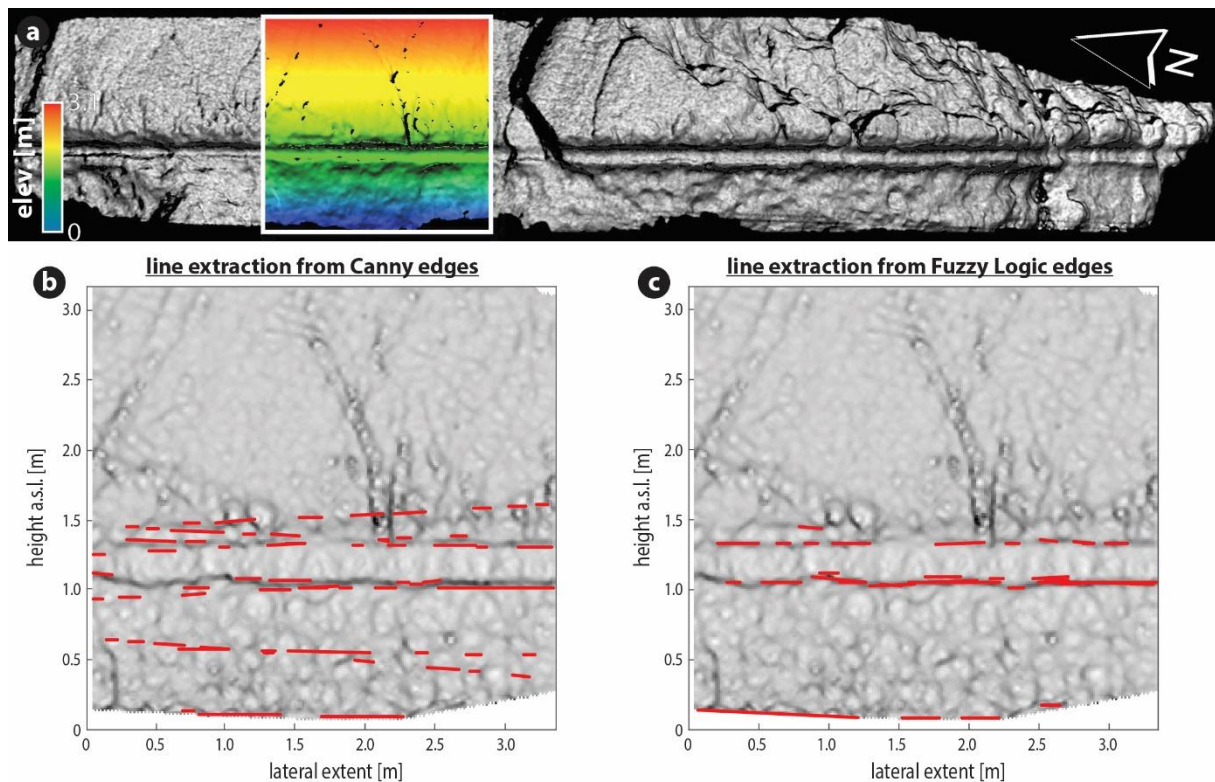


Fig. 8. Feature extraction from scan of the cliff at Agios Pavlos. a) Overall result. b) Extracted line objects from Canny edges. c) Objects from Fuzzy logic edge detection representing the sea-level marker more concentrated along the notch extent line.

4.2. Testing methods, Perachora Peninsula, eastern Gulf of Corinth

The entire workflow was tested at different sites along the coast of the Perachora Peninsula. This setting has been extensively studied due to the 1981 earthquake sequence that attracted several research groups, and Holocene tidal notches have been described. Kershaw and Guo (2001) recognised five different notch generations (~ 2.7 , ~ 2 , ~ 1.2 , ~ 0.4 , and 0 m) at Mylokopy Bay (see Fig. 1b). Laser scan data, covering an area of almost 6.5×3.8 m of the cliff, was processed for curvature analysis. Line feature extraction from Hough transformation confirmed evidence for all five levels (Fig. 9a). Obviously, edges from the Canny detector result in many more line features across the scan than from the Fuzzy logic approach. Canny edges produce line structures almost evenly spread from $\sim +1$ m up to the top of the scan window. Only insignificant line features are determined for the lower most part of the scan data. A confirmation of published indentations is only possible because of their known extents. Furthermore, the recently developing notch is only evidenced by Fuzzy logic edges. Thus, Canny edges indicate remnants of tidal notches but are accompanied by noise which is the result of morphological structures of minor significance. Due to the significant number of extracted lines from Canny edges it is hard to identify distinct levels. Also, line orientation is predominantly not horizontal but showing slight inclined trends although only features of $\vartheta > 80^\circ$ are considered. Structures from Fuzzy logic edges appear much more horizontal. It is noticeable that even Fuzzy logic edge detection method produces line features of considerable length that do not belong to any of the published notch morphologies, yet are located between two published notch levels ($+2.4$ m).

Similar results can be noticed for both sites at Heraion. Kershaw and Gou (2001) identified two notches at the southern part of the Harbour and correlated them to four notches determined by Pirazzoli et al. (1994). The output for both sites supports the potential of tidal notch detection from Fuzzy logic edges. Lower parts at the Heraion harbour site are significantly rougher than from the rest of the scan and produce line structures without significant cluster levels. A horizontal and convex morphology ~2 m a.s.l. evidences the remnant of a notch roof (Fig. 9b). Its remains are poorly preserved and only a few line features are extracted from Fuzzy logic edges. However, a conventional 2D profile supports its existence. A notch at +1.8 m in between both published notches might represent a so far unrecognised earthquake event.

At the cliff beneath the lighthouse, Canny edges only produce poor results (Fig. 9c). There is only one evidence for a notch provided as a line feature at ~1 m. This feature matches to a convex edge that might represent the roof of a so far unpublished notch just below the lowermost notch identified by Pirazzoli et al. (1994) at +1.1 m (see also Fig. 1d). It is worth noting that the roof corresponding to the notch at +1.1 m was missed by the Canny algorithm. Contrastingly, Fuzzy logic edges provide evidence for the roofs (+3.5, +3.0, +2.0, and +1.3 m) of all four published notches at corresponding heights (inferred mean sea-levels at ~3.2, ~2.6, ~1.7, and ~1.1 m). However, there is also evidence for a further notch roof at ~2.4 m in between two recognised notch horizons. This evidence is supported by both edge inputs following same parameters in the Hough transform and the 2D profile (Fig. 9c).

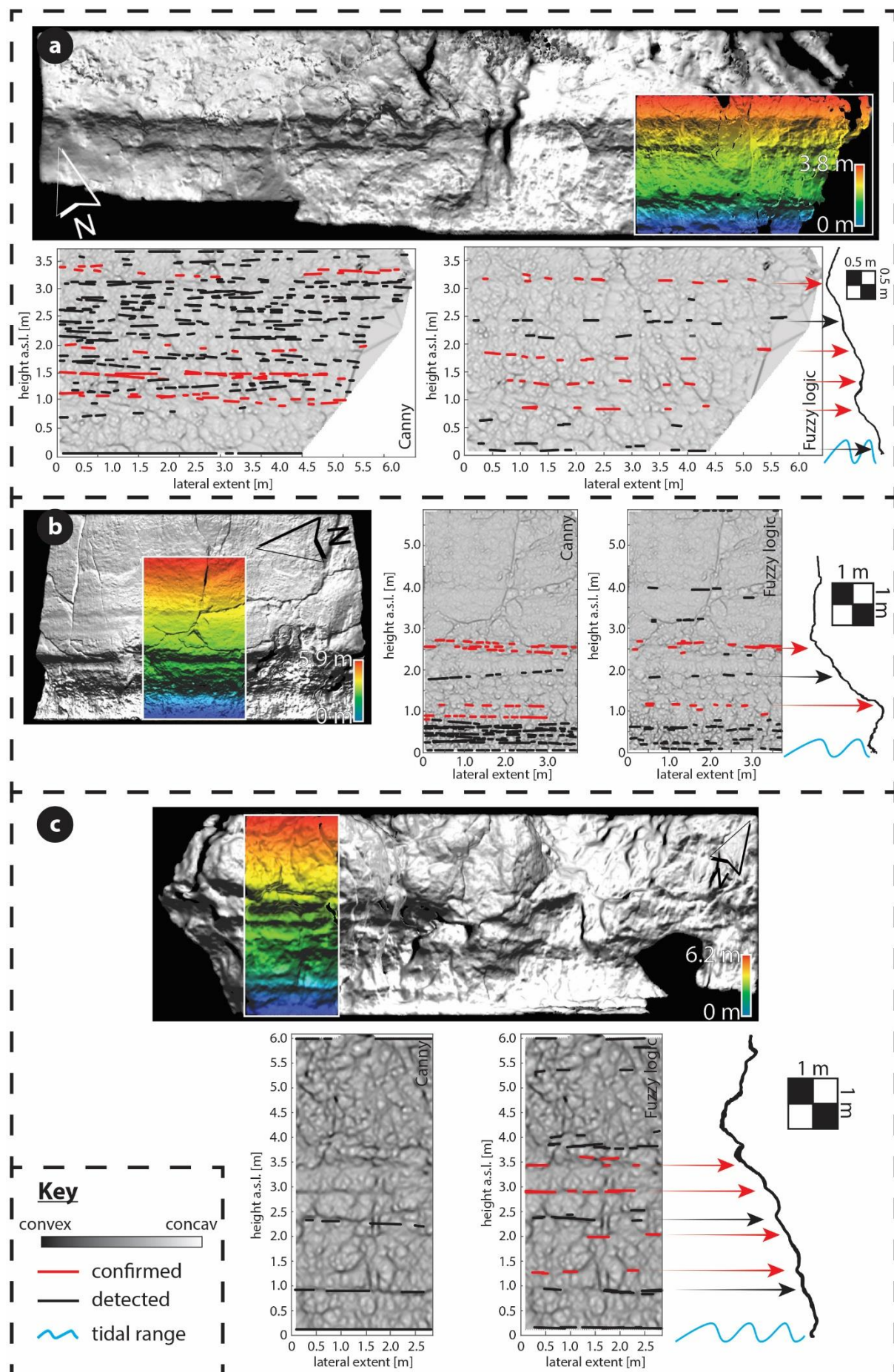


Fig. 9. Results of testing methods along coast of the Perachora Peninsula. The locations of investigated data in each scan are indicated colourising the height levels. Published notches are provided and correlated to the results of line extraction at Mylokopy bay (a), Heraion harbour site (b), and Heraion Lighthouse site (c). Red arrows indicate the position of the roof of known notches. Black arrows point at morphological characteristics that could correspond to new notches.

5. Discussion and concluding remarks

TLS is a commonly used technique for morphological purposes (e.g. Rosser et al., 2014; Wilkinson et al., 2015). Due to its flexibility, quality, and accuracy, the resulting data highlights even minor evidence of spatial peculiarities. In this study, the detailed examination of tidal notches preserved owing to tectonic activity and coastal uplift has been undertaken. Thereby, uplift values in the order of a few decimetres are expected in extensional settings (Papanikolaou et al., 2010) and therefore, a high spatial resolution is required and this is offered by the TLS. Furthermore, a mesoscale downward widening of pre-existing tidal notches is likely. The former notch floor as well as biological markers, such as *Lithophaga* agents, could be overprinted by the newer tidal notch generation. Thus minor but horizontally consistent changes in the surfaces' curvature might be evidence for sea-level indicators that were eroded along their lower extent over time, or did not have enough time to develop because of short recurrence intervals between uplift events. Thereby, the local tidal amplitude (here: 0.2 m) forms the resolution limit. Traditional profiling with tape measures or laser distance meter (Kázmér and Taboroší, 2012) aims to identify tidal notches from a digital copy of the vertical cliff topography. When corrected for sea-level datum, information about elevation and notch dimensions can be inferred. This includes both horizontal and vertical extent per feature (Pirazzoli, 1986). Multiple profiles can only be correlated when referring to the same datum. However, spatial variations in cliff topography of closely positioned sites are hard to verify from horizontally stacked 2D profiles, as a consequence of bedrock heterogeneity, local variations of wave action, and/or fault movements (Kershaw and Guo, 2001). Utilising TLS measurements in notch studies presents the opportunity to collect high resolution spatial data from exposures (even from distance) in a rectified manner, which is not possible using conventional tape measurement or photogrammetry and SfM approaches (Bini et al., 2014). Even submerged notches down to 0.8 m are not excluded from TSL surveys when using systems operating at the green-wavelength (Smith, 2015).

The presented workflow aims to detect the roof and/or floor of raised tidal notches by reducing spatial information and focussing on horizontal continuities. Convex patterns, pointing towards the sea, pose evidence for remnants of tidal notches (see Fig. 3). The principal curvature analysis highlights such patterns but does not link those to the attributes of two-dimensional orientation or continuity. However, the magnitude of curvature can be utilised to describe significant morphological changes. Such information is input data for edge detection analysis. Herein, two methods of edge detection were tested in order to reduce spatial information towards its varying significance. In computer vision and image processing, the Canny edge detector algorithm depicts a standard operator (Bao et al., 2005) for tracking ridges in gradient magnitude images (Canny, 1986). A disadvantage of this method is that all extracted edges appear to have the same significance (see Fig. 6b). Thus, edges in areas of minor interest and oriented both vertically and horizontally, appear the same as those of relevance for tidal notch detection. Therefore, a Fuzzy logic sequence was constructed comprising of membership functions that enable exclusive focus on significant horizontal changes in surface curvature. Even if the

input information is incomplete or imprecise, the approach outputs predominantly continuous and horizontally oriented structures. Instead of crisp boundaries between two classes (e.g. edge or uniform), the membership functions are defined to give probabilistic information on edge existence (see Fig. 6c). However, resulting edge information from both algorithms were individually used as input data for the final Hough transform, which intends to extract continuous line features. Missing points on the desired curves as well as spatial variations between the ideal line and the noise edge points are the result of imperfections in either the image data or the applied edge detection algorithm. The Hough transform produces discrete parameter space matrices of the spatial data in which voting peaks indicate a continuous line object. Furthermore, minor restrictions to the objects orientation yield in spatial matching of identified lines and tidal notch extents (see Fig. 8). The ability to adjust the edge detection algorithm for individual requirements, using a Fuzzy logic approach appears to be more reliable for highlighting notch morphologies than the Canny edge detection. Due to the possibility of excluding plan changing curvature and defining membership grades, the line objects extracted from Fuzzy logic edge detection is most suitable.

As mentioned above edge detection and line object extraction target remnants of raised notches, such as their roof and/or floor. This should not be confused with the aims of traditional cliff profiling. Here, the depth of a notch is not analysed and thus the outcome does not allow any conclusion on the developing period as a function of the erosion rate. Only the vertical extent is measurable if the notch is completely preserved. In Agios Pavlos, it is possible to obtain estimates of the tidal range ($\sim 0.35 \pm 0.05$ m) which are consistent with estimates from Evelpidou et al. (2012). However, assuming a constant local tidal range throughout the Holocene allows the projection of the historic mean sea-levels with half the erosive zone beneath the detected roof and half above the detected floor, respectively. Hence, historic sea-levels can be reconstructed although the majority of their morphological footprints in a coastal cliff are no longer existent. Furthermore, data collection via TLS enables the extraction of multiple traditional profiles easily for conventional analyses as well (see profiles in Fig. 1) and adds coherent information on the third dimension to address local heterogeneities. Therefore, traditional and presented approaches validate and complete each other from the same data base.

Palaeoseismological studies are frequently assisted by tidal notch investigations in areas of coastal tectonic activity (e.g. Kershaw and Guo, 2001). In particular, in extensional tectonic settings the footwall coastal uplift is not likely to exceed several decimetres (e.g. Papanikolaou et al., 2010). However, Pirazzoli et al. (1994) identified a series of four tidal notches of Holocene age at Heraion (Fig. 1d), each displaced by repeated uplifts of about 0.8 ± 0.3 m. Assuming a ratio of 1/4 net slip per event, this would equate to 4 m total offset in an area where Jackson et al. (1982) reported just minor coseismic uplift of 0.2 during the Alkyonides earthquake sequence (M 6.4–6.7) in February and March 1981. If evidence for remnants of tidal notches in between more distinct features are detected by using high resolution data in high performance algorithms, palaeomagnitude estimates get more realistic. For instance, both Canny and Fuzzy logic edges provided evidence for notch roofs at +1.0 and +2.4 m at the cliff beneath the lighthouse, respectively. These positions fit in the idea of regular displacements during earthquakes and reduce mean notch offset yielding reliable values of coseismic uplift (0.5 ± 0.2 m per event). A second example is obtained at Mylokopy. Including additional notch roofs (~ 0.6 , ~ 1.3 , and ~ 2.25 m) would result in repeated uplifts of about 0.4 ± 0.18 m corresponding to magnitudes of M 6.7 ± 0.1 in accordance with Wells and Coppersmith (1994). The results help to reconcile the discrepancy between the palaeoseismic record and the direct observations of co-seismic

displacements provided by Jackson et al. (1982). Minor but horizontally continuous remnants revealed by dense point cloud data are usually not validated in single 2D profiles. However, the identification of new notch levels would (partially) solve the paradox between large tectonic uplift values and plausible palaeomagnitudes.

The results show the possibility of tidal notch detection by curvature analysis and subsequent edge detection and line feature extraction. It is shown that morphologies accepted as tidal notches can be detected by reducing high resolution point cloud data towards the principal curvature pointing at the roof or the floor of a notch, respectively (see Figs. 8c and 9b). Even evidence for previously unidentified structures are extracted from the data. As a consequence more realistic uplift values would result if these features get proven as remnants of tidal notches. The workflow enables the objective validation of observations along coastline by evaluating coastal cliffs in three dimensions. Therefore, reliable statements on coast uplifting earthquake events are possible. The variability of conventionally collected tidal notch profiles (Kershaw and Guo, 2001) is circumvented by instant 3D data collection in high resolution and applied spatial analytics. Furthermore, the semi-automated workflow provides fast results once adjusted for individual needs. The benefits are as follows:

- Enhanced objectivity in recognising tidal notch morphologies on cliff faces.
- More insights from high-resolution 3D TLS by recognising undiscovered notches or features corresponding to multiple notches.
- Valuable information on morphological characteristics even of only minor distinction and their spatial distribution especially in extensional tectonic settings, where coseismic uplift is much less than in compressional environments.

However, data quality and thus the reliability of the outcome remain dependent on the preservation of individual tidal notches on a coastal cliff. Sheltered sites in microtidal seas provide perfect conditions for tidal notch preservation after emergence whereas inhomogeneous and disturbed cliffs exposed to the open sea (Pirazzoli, 1986) are not likely to be good archives of Holocene earthquake events. Furthermore, varying bedrock consistency or the presence of bedding planes may yield in the formation of minor structural notches. Especially when the bedding is horizontally oriented, misinterpretation by remote morphological analysis cannot be neglected (Kershaw and Guo, 2001). This implies that along coast a natural variance of tidal notches masked by surf processes and inhomogeneities yields different results of tidal notch identification. Therefore, careful site selection for palaeo-shoreline identification should consider constraints of marine attacks, tectonic influences on- and offshore and coastal geology. In order to consider such local lateral variations, 3D data acquisition helps to reduce sources of misinterpretation. Therefore, we show that TLS combined with up to date post-processing edge analyses can form a rigorous and useful approach to the interpretation of palaeoseismic records from Holocene tidal notches.

Acknowledgements

Hellenic Navy Hydrographic Service (HNHS) provided sea-level data from the Posidonia station. Thanks to C. Hilgers and his team (RWTH Aachen University) for the loan of the TLS system. T. M. Fernández-Steeger (RWTH Aachen University) is acknowledged for financial support and fruitful discussions. Miklos Kázmér (Eötvös University, Budapest) is acknowledged for his assistance in the field. We are

grateful to Luigi Ferranti and an anonymous reviewer as well as to Editor Takashi Oguchi for their useful and improving suggestions on our manuscript.

References

Antonioli, F.; Lo Presti, V.; Rovere, A.; Ferranti, L.; Anzidei, M.; Furlani, S.; Mastronuzzi, G.; Orru, P.E.; Scicchitano, G.; Sannino, S.; Spampinato, C.R.; Palgiarulo, R.; Deiana, G.; de Sabata, E.; Sansó, P.; Vacchi, M.; Vecchio, A. (2015): Tidal notches in Mediterranean Sea: a comprehensive analysis. In *Quaternary Science Reviews* 119, pp. 66–84. DOI: 10.1016/j.quascirev.2015.03.016.

Armijo, R.; Meyer, B.; King, G. C. P.; Rigo, A.; Papanastassiou, D. (1996): Quaternary evolution of the Corinth Rift and its implications for the Late Cenozoic evolution of the Aegean. In *Geophysical Journal International* 126 (1), pp. 11–53. DOI: 10.1111/j.1365-246X.1996.tb05264.x.

Bao, P.; Zhang, L.; Wu, X. (2005): Canny edge detection enhancement by scale multiplication. In *IEEE transactions on pattern analysis and machine intelligence* 27 (9), pp. 1485–1490. DOI: 10.1109/TPAMI.2005.173.

Bellman, R. E.; Zadeh, L. A. (1970): Decision-Making in a fuzzy environment. In *Management science* 17 (4), pp. B-141 - B-164.

Bezdek, J. C.; Harris, J. D. (1978): Fuzzy Partitions and Relations; an axiomatic basis for clustering. In *Fuzzy Sets and Systems* 1, pp. 111–127.

Bini, M.; Isola, I.; Pappalardo, M.; Ribolini, A.; Favalli, M.; Ragaini, L.; Zanchetta, G. (2014): Abrasive notches along the Atlantic Patagonian coast and their potential use as sea level markers: the case of Puerto Deseado (Santa Cruz, Argentina). In *Earth Surf. Process. Landforms*, pp. n/a. DOI: 10.1002/esp.3612.

Bonneau, M. (1985): 1:50.000 Geological Map Sheet Melambes, Institute of Geology and Mineral Exploration (IGME).

Bornovas, J.; Gaitanakis, P.; Spiridopoulos, A. (1984): 1:50.000 Geological Map Sheet Perachora, Institute of Geology and Mineral Exploration (IGME).

Boulton, S. J.; Stewart, I. S. (2015): Holocene coastal notches in the Mediterranean region: Indicators of palaeoseismic clustering? In *Geomorphology* 237, pp. 29–37. DOI: 10.1016/j.geomorph.2013.11.012.

Canny, J. (1986): A Computational Approach to Edge Detection. In *IEEE Trans. Pattern Anal. Mach. Intell.* PAMI-8 (6), pp. 679–698. DOI: 10.1109/TPAMI.1986.4767851.

Caputo, R.; Catalano, S.; Monaco, C.; Romagnoli, G.; Tortorici, G.; Tortorici, L. (2010): Active faulting on the island of Crete (Greece). In *Geophysical Journal International* 183 (1), pp. 111–126. DOI: 10.1111/j.1365-246X.2010.04749.x.

616 Collier, R. E. L.; Leeder, M. R.; Rowe, P. J.; Atkinson, T. C. (1992): Rates of tectonic uplift in the Corinth
617 and Megara Basins, central Greece. In *Tectonics* 11 (6), pp. 1159–1167. DOI: 10.1029/92TC01565.

618 Cooper, F. J.; Roberts, G. P.; Underwood, C. J. (2007): A comparison of 10³–10⁵ year uplift rates on
619 the South Alkyonides Fault, central Greece: Holocene climate stability and the formation of coastal
620 notches. In *Geophys. Res. Lett.* 34 (14). DOI: 10.1029/2007GL030673.

621 Cowie, P. A.; Roberts, G. P. (2001): Constraining slip rates and spacings for active normal faults. In
622 *Journal of Structural Geology* 23 (12), pp. 1901–1915. DOI: 10.1016/S0191-8141(01)00036-0.

623 Duda, R. O.; Hart, P. E. (1972): Use of the Hough Transformation to detect lines and curves in pictures.
624 In *Comm. ACM.* 15 (1), pp. 11–15.

625 Evelpidou, N.; Kampolis, I.; Pirazzoli, P. A.; Vassilopoulos, A. (2012): Global sea-level rise and the
626 disappearance of tidal notches. In *Global and Planetary Change* 92–93, pp. 248–256. DOI:
627 10.1016/j.gloplacha.2012.05.013.

628 Fernandes, L. A.F.; Oliveira, M. M. (2008): Real-time line detection through an improved Hough
629 transform voting scheme. In *Pattern Recognition* 41 (1), pp. 299–314. DOI:
630 10.1016/j.patcog.2007.04.003.

631 Jackson, J. A.; Gagnepain, J.; Houseman, G.; King, G.C.P.; Papadimitriou, P.; Soufleris, C.; Virieux, J.
632 (1982): Seismicity, normal faulting, and the geomorphological development of the Gulf of Corinth
633 (Greece): the Corinth earthquakes of February and March 1981. In *Earth and Planetary Science Letters*
634 57 (2), pp. 377–397. DOI: 10.1016/0012-821X(82)90158-3.

635 Jones, R. R.; Kokkalas, S.; McCaffrey, K.J.W. (2009): Quantitative analysis and visualization of nonplanar
636 fault surfaces using terrestrial laser scanning (LIDAR)--The Arkitsa fault, central Greece, as a case study.
637 In *Geosphere* 5 (6), pp. 465–482. DOI: 10.1130/GES00216.1.

638 Kázmér, M.; Taboroši, D. (2012): Rapid Profiling of Marine Notches Using a Handheld Laser Distance
639 Meter. In *Journal of Coastal Research* 283, pp. 964–969. DOI: 10.2112/JCOASTRES-D-11-00163.1.

640 Kershaw, S.; Guo, L. (2001): Marine notches in coastal cliffs: indicators of relative sea-level change,
641 Perachora Peninsula, central Greece. In *Marine Geology* 179 (3–4), pp. 213–228. DOI: 10.1016/S0025-
642 3227(01)00218-3.

643 Laborel, J.; Morhange, C.; Collina-Girard, J.; Laborel-Deguen, F. (1999): Littoral bioerosion, a tool for
644 the study of sea level variations during the Holocene. In *Bulletin of the Geological Society of Denmark*
645 45, pp. 164–168.

646 Leeder, M. R.; McNeill, L. C.; LI Collier, R. E.; Portman, C.; Rowe, P. J.; Andrews, J. E.; Gawthorpe, R. L.
647 (2003): Corinth rift margin uplift: New evidence from Late Quaternary marine shorelines. In *Geophys.*
648 *Res. Lett.* 30 (12), pp. n/a. DOI: 10.1029/2003GL017382.

649 Leeder, M. R.; Portman, C.; Andrews, J. E.; Collier, R.E.LI.; Finch, E.; Gawthorpe, R. L. et al. (2005):
650 Normal faulting and crustal deformation, Alkyonides Gulf and Perachora peninsula, eastern Gulf of
651 Corinth rift, Greece. In *Journal of the Geological Society* 162 (3), pp. 549–561. DOI: 10.1144/0016-
652 764904-075.

Liberti, L.; Carillo, A.; Sannino, G. (2013): Wave energy resource assessment in the Mediterranean, the Italian perspective. In *Renew. Energy* 50, pp. 938–949. Available online at <http://utmea.enea.it/projects/energiadalmare/index.php>.

Krijgsman, W. (1996): Miocene magnetostratigraphy and cyclostratigraphy in the Mediterranean. Extension of the astronomical polarity time scale. [Utrecht]: [Faculteit Aardwetenschappen, Universiteit Utrecht] (Geologica Ultraiectina, no. 141).

McNeill, L. C.; Collier, R.E.Ll. (2004): Uplift and slip rates of the eastern Eliki fault segment, Gulf of Corinth, Greece, inferred from Holocene and Pleistocene terraces. In *Journal of the Geological Society* 161 (1), pp. 81–92. DOI: 10.1144/0016-764903-029.

McNeill, L. C.; Cotterill, C. J.; Henstock, T. J.; Bull, J. M.; Stefatos, A.; Collier, R.E.Ll.; Papatheoderou, G.; Ferentinos, G.; Hicks, S.E. (2005): Active faulting within the offshore western Gulf of Corinth, Greece: Implications for models of continental rift deformation. In *Geol* 33 (4), p. 241. DOI: 10.1130/G21127.1.

Meulenkamp, J. E.; van der Zwaan, G.J.; van Wamel, W. A. (1994): On late miocene to recent vertical motions in the Cretan segment of the Hellenic arc. In *Tectonophysics* 234 (1-2), pp. 53–72. DOI: 10.1016/0040-1951(94)90204-6.

Morewood, N. C.; Roberts, G. P. (1999): Lateral propagation of the surface trace of the South Alkyonides normal fault segment, central Greece: its impact on models of fault growth and displacement–length relationships. In *Journal of Structural Geology* 21 (6), pp. 635–652. DOI: 10.1016/S0191-8141(99)00049-8.

Otsu, N. (1979): A Threshold Selection Method from Gray-Level Histograms. In *IEEE Trans. Syst., Man, Cybern.* 9 (1), pp. 62–66. DOI: 10.1109/TSMC.1979.4310076.

Papanikolaou, D. J.; Royden, L. H. (2007): Disruption of the Hellenic arc: Late Miocene extensional detachment faults and steep Pliocene-Quaternary normal faults-Or what happened at Corinth? In *Tectonics* 26 (5), pp. n/a. DOI: 10.1029/2006TC002007.

Papanikolaou, I. D.; Fouvelis, M.; Parcharidis, I.; Lekkas, E. L.; Fountoulis, I. G. (2010): Deformation pattern of the 6 and 7 April 2009, $M_W=6.3$ and $M_W=5.6$ earthquakes in L'Aquila (Central Italy) revealed by ground and space based observations. In *Nat. Hazards Earth Syst. Sci.* 10 (1), pp. 73–87. DOI: 10.5194/nhess-10-73-2010.

Pirazzoli, P. A. (1986): Marine notches. In Orson van de Plassche (Ed.): *Sea-Level Research*. Dordrecht: Springer Netherlands, pp. 361–400.

Pirazzoli, P. A. (1991): *World atlas of Holocene sea-level changes*. Amsterdam, New York: Elsevier (Elsevier oceanography series, 58).

Pirazzoli, P. A.; Stiros, S. C.; Arnold, M.; Laborel, J.; Laborel-Deguen, F.; Papageorgiou, S. (1994): Episodic uplift deduced from Holocene shorelines in the Perachora Peninsula, Corinth area, Greece. In *Tectonophysics* 229 (3-4), pp. 201–209. DOI: 10.1016/0040-1951(94)90029-9.

Pirazzoli, P. A.; Evelpidou, N. (2013): Tidal notches: A sea-level indicator of uncertain archival trustworthiness. In *Palaeogeography, Palaeoclimatology, Palaeoecology* 369, pp. 377–384. DOI: 10.1016/j.palaeo.2012.11.004.

691 Roberts, G. P.; Houghton, S. L.; Underwood, C.; Papanikolaou, I.; Cowie, P. A.; van Calsteren, P.; Wigley,
692 T.; Cooper, F.J.; McArthur, J.M. (2009): Localization of Quaternary slip rates in an active rift in 10 5
693 years: An example from central Greece constrained by 234 U- 230 Th coral dates from uplifted
694 paleoshorelines. In *J. Geophys. Res.* 114 (B10). DOI: 10.1029/2008JB005818.

695 Rosser, N. J.; Brain, M. J.; Petley, D. N.; Lim, M.; Norman, E. C. (2013): Coastline retreat via progressive
696 failure of rocky coastal cliffs. In *Geology* 41 (8), pp. 939–942. DOI: 10.1130/G34371.1.

697 Schneiderwind, S.; Mason, J.; Wiatr, T.; Papanikolaou, I.; Reicherter, K. (2016): 3-D visualisation of
698 palaeoseismic trench stratigraphy and trench logging using terrestrial remote sensing and GPR – a
699 multiparametric interpretation. In *Solid Earth* 7 (2), pp. 323–340. DOI: 10.5194/se-7-323-2016.

700 Shaw, B.; Ambraseys, N. N.; England, P. C.; Floyd, M. A.; Gorman, G. J.; Higham, T. F. G. et al. (2008):
701 Eastern Mediterranean tectonics and tsunami hazard inferred from the AD 365 earthquake. In *Nature*
702 *Geosci* 1 (4), pp. 268–276. DOI: 10.1038/ngeo151.

703 Smith, M. W. (2015): Direct acquisition of elevation data: Terrestrial Laser Scanning. Edited by British
704 Society for Geomorphology. *Geomorphological Techniques*, Chp. 2, Sec. 1.5.

705 Stewart, I.; Vita-Finzi, C. (1996): Coastal uplift on active normal faults: The Eliki Fault, Greece. In
706 *Geophys. Res. Lett.* 23 (14), pp. 1853–1856. DOI: 10.1029/96GL01595.

707 Stiros, S. C. (2010): The 8.5+ magnitude, AD365 earthquake in Crete: Coastal uplift, topography
708 changes, archaeological and historical signature. In *Quaternary International* 216 (1-2), pp. 54–63. DOI:
709 10.1016/j.quaint.2009.05.005.

710 Trenhaile, A. S. (2015): Coastal notches: Their morphology, formation, and function. In *Earth-Science*
711 *Reviews* 150, pp. 285–304. DOI: 10.1016/j.earscirev.2015.08.003.

712 Wells, D.L.; Coppersmith, K.J. (1994): New Empirical Relationships among Magnitude, Rupture Length,
713 Rupture Width, Rupture Area, and Surface Displacement. In *Bulletin of the Seismological Society of*
714 *America*, 84 (4), pp. 974-1002.

715 Wiatr, T.; Papanikolaou, I.; Fernández-Steeger, T.; Reicherter, K. (2015): Bedrock fault scarp history:
716 Insight from t-LiDAR backscatter behaviour and analysis of structure changes. In *Geomorphology* 228,
717 pp. 421–431. DOI: 10.1016/j.geomorph.2014.09.021.

718 Wilkinson, M.; Roberts, G. P.; McCaffrey, K.; Cowie, P. A.; Faure Walker, J. P.; Papanikolaou, I.; Phillips,
719 R.J.; Michetti, A.M.; Vittori, E.; Gregory, L.; Wedmore, L.; Watson, Z.K. (2015): Slip distributions on
720 active normal faults measured from LiDAR and field mapping of geomorphic offsets: an example from
721 L'Aquila, Italy, and implications for modelling seismic moment release. In *Geomorphology* 237,
722 pp. 130–141. DOI: 10.1016/j.geomorph.2014.04.026.

723 Zadeh, L. A. (1965): Fuzzy Sets. In *Information and Control* 8, pp. 338–353.

724 Zhang, H.; Zhu, Q.; Fan, C.; Deng, D. (2013): Image quality assessment based on Prewitt magnitude. In
725 *AEU - International Journal of Electronics and Communications* 67 (9), pp. 799–803. DOI:
726 10.1016/j.aeeu.2013.04.001.

727